Effects of Sulfur Site Modification on the Redox Potentials of Derivatives of [*N*,*N*′-Bis(2-mercaptoethyl)-1,5-diazacyclooctanato]nickel(II)

Patrick J. Farmer, Joseph H. Reibenspies, Paul A. Lindahl, and Marcetta Y. Darensbourg*

Contribution from the Department of Chemistry, Texas A&M University, College Station, Texas 77843

Received October 15, 1992

Abstract: Cyclic voltammetry has been used to examine $Ni^{II/I}$ and $Ni^{II/III}$ redox potential data for a structurally characterized homologous series of six NiN_2S_2 complexes, in which the sulfur sites are systematically varied in donor ability: thiolate (RS^-), thioether (RSR), sulfinate (RSO_2^-), and mixtures of these. These include [*N*,*N*′-bis(mercaptoethyl)-1,5-diazacyclooctanato]nickel(II) ((bme-daco)Ni^{II}, **1**), [*N*-(mercaptoethyl)-*N*′-(sulfinoethyl)-1,5-diazacyclooctanato]nickel(II) ((mese-daco)Ni^{II}, **2**), [*N*,*N*′-bis(sulfinoethyl)-1,5-diazacyclooctanato]nickel(II) ((bse-daco)Ni^{II}, **3**), [*N*-(mercaptoethyl)-*N*′-(3-thiabutyl)-1,5-diazacyclooctanato]nickel(II) iodide ([(metb-daco)Ni][I], **4**), [*N*-(sulfinoethyl)-*N*′-(3-thiabutyl)-1,5-diazacyclooctanato]nickel(II) iodide ([(setb-daco)Ni][I], **5**), and [*N*,*N*′-bis(3-thiabutyl)-1,5-diazacyclooctane]nickel(II) diiodide ([(btb-daco)Ni][I]$_2$, **6**). X-ray crystallography has established that all complexes are largely square planar with distortions toward tetrahedral ranging from 1° (strictly square planar) to 18.3°. Throughout the series, the differences in Ni–S bond distances vary <0.08 Å, with the shortest distance at 2.133(3) Å for Ni–SO_2R in **3** and the longest distance at 2.211(3) Å for Ni–SR_2 in **6**. All complexes show reversible reduction waves in CH_3CN, assigned to the $Ni^{II/I}$ couple in complexes **2–6** by EPR of chemically reduced solutions. The $Ni^{II/I}$ potentials vary over a ca. 1.5-V range. Within the series the Ni^I state is most accessible (–482 mV vs NHE in CH_3CN) for the dithioether complex (**6**) and least for the dithiolate (**1**). Changes in the donor character of the sulfur ligands have a consistent and additive effect on the redox potentials: in CH_3CN each methylation of the nickel-bound thiolates results in stabilization of Ni^I by ca. 700 mV whereas each oxygenation stabilizes the $Ni^{II/I}$ couple ca. 300 mV. Potential measurements in water demonstrate large hydrogen-bonding effects for the complexes with thiolate and sulfinate donor sites. Reversible $Ni^{II/III}$ couples are observed only for complexes **3** and **6**. For all complexes the separation between reduction and oxidation events is ca. 2 V. The crystal structure is given of previously reported (bse-daco)Ni^{II} (**3**), which crystallizes in the orthorhombic $P2_12_12$ (No. 18) space group with a = 8.696(4) Å, b = 9.993(5) Å, c = 8.015(4) Å, V = 696.5(5) Å^3, and Z = 2. The synthesis and structure of two new compounds are given: [(metb-daco)Ni^{II}][I] (**4**) crystallizes in the triclinic $P\bar{1}$ (No. 2) space group with a = 7.558(5) Å, b = 8.922(7) Å, c = 12.559(9) Å, α = 102.79(6)°, β = 95.05(6)°, γ = 107.23(6)°, V = 778.0(10) Å^3, and Z = 2; and [(setb-daco)Ni^{II}][I] (**5**) crystallizes in the monoclinic $P2_1/n$ (No. 14) space group with a = 9.012(2) Å, b = 12.891(3) Å, c = 14.055(3) Å, β = 99.42(2)°, V = 1610.8(6) Å^3, and Z = 4.

Questions regarding the mechanism of the catalytic cycle in [NiFe] hydrogenases revolve about the redox potential of nickel in a classical ligand (N (O), S (Cl)) donor site environment. Biomodeling has been faced with the problem of providing structural models with redox potentials consistent with the chemistry of two cycles: (1) the activation of an inactive form, widely interpreted as Ni^{III}, with an impressively low $Ni^{III/II}$ couple (–150 to –400 mV vs NHE), and (2) the $H_2/2H^+$ catalytic cycle involving an active form presumed to be $Ni^{II/I}$ in character.[1] The conflict in this task is that ligation factors which stabilize Ni^I and Ni^{III} oxidation states are typically different[2] and model systems that achieve stabilization of both odd oxidation states of nickel show a difference between $Ni^{III/II}$ and $Ni^{II/I}$ couples of about 2 V,[3] rather than a few hundred millivolts as is seen for Ni hydrogenases.[1]

Despite impressive synthetic successes, structural, electrochemical, and functional models which are simultaneously satisfactory for both portions of the process have yet to be demonstrated. The available models are usually based on strongly binding multidentate ligands deemed necessary to retain the oxidized or reduced form of nickel within the complex.[4–7] Efforts to mimic the low $Ni^{III/II}$ couple have centered on tetraanionic ligands; Holm et al. have critically reviewed the ligand systems (amide, oxime, thiocarbonate, and thiolate) which achieve Ni^{III} at biologically accessible potentials.[4] Thus far, however, hydrogenase activity such as H/D exchange has been displayed only by models which have accessible Ni^I states.[8] A recent study has demonstrated the similarity of Ni^I EPR signals to the Ni signal associated with the active catalyst cycle of the *T. roseopersicina* hydrogenase.[7b]

Systematic studies of the effect of macrocyclic ring size, alkyl substituents on the ligand framework, and degree of conjugation in tetraaza macrocycles on Ni redox behavior are available and illustrate additivity in the ligand structural changes on electrode

(1) (a) Cammack, R.; Fernandez, V. M.; Schnieder, K. *The Bioinorganic Chemistry of Nickel*; Lancaster, J. R., Ed.; VCH Publishers: New York, 1988; Chapter 4. (b) Moura, J. J. G.; Texiera, M.; Moura, I.; LeGall, J. *The Bioinorganic Chemistry of Nickel*; Lancaster, J. R., Ed.; VCH Publishers: New York, 1988; Chapter 9. (c) Cammack, R. *Adv. Inorg. Chem.* **1988**, *32*, 297.

(2) Nag, K.; Chakravorty, A. *Coord. Chem. Rev.* **1980**, *33*, 87.

(3) Lovecchio, F. V.; Gore, E. S.; Busch, D. H. *J. Am. Chem. Soc.* **1974**, *96*, 3109. Busch, D. H. *Acc. Chem. Res.* **1978**, *11*, 392.

(4) Krüger, H.-J.; Peng, G.; Holm, R. H. *Inorg. Chem.* **1991**, *30*, 734.

(5) Colpas, G. J.; Kumar, J.; Day, R. O.; Maroney, M. J. *Inorg. Chem.* **1990**, *29*, 4779.

(6) Fox, S.; Wang, Y.; Silver, A.; Millar, M. *J. Am. Chem. Soc.* **1990**, *112*, 3218.

(7) (a) Baidya, N.; Olmstead, M.; Mascharak, P. K. *Inorg. Chem.* **1991**, *30*, 929. (b) Baidya, N.; Olmstead, M. M.; Whitehead, J. P.; Bagyinka, C.; Maroney, M. J.; Mascharak, P. K. *Inorg. Chem.* **1992**, *31*, 3612. (c) Baidya, N.; Olmstead, M. M.; Mascharak, P. K. *J. Am. Chem. Soc.* **1992**, *114*, 9666.

(8) Zimmer, M.; Schulte, G.; Luo, X. L.; Crabtree, R. H. *Angew. Chem., Int. Ed. Eng.* **1991**, *30*, 193.

0002-7863/93/1515-4665$04.00/0

Scheme I

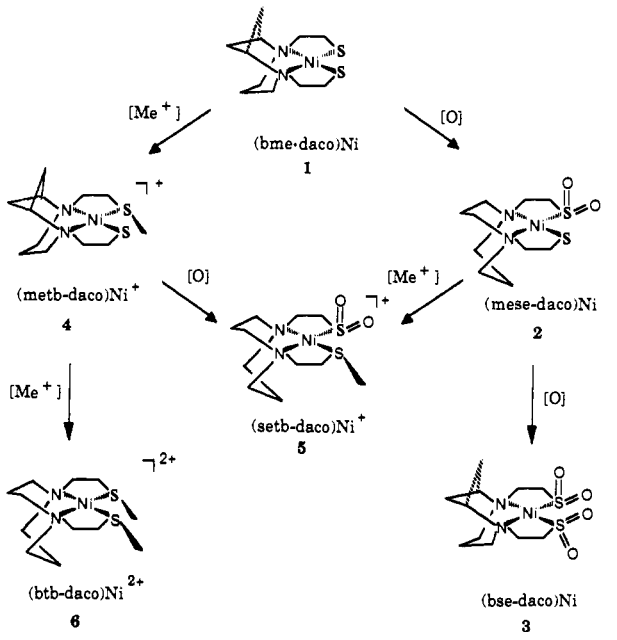

potentials.[3] The effect of sulfur donors on the potentials of nickel redox activity are less codified, despite considerable evidence for the "softening" character of the π-accepting thioether-S donor as contrasted to the good π-donor thiolate ligand.[9] Since both are possible biological ligands in the forms of methionine and cysteinate, respectively, a quantitative basis for predicting the effect of such S-donors on electrochemistry would be useful.

We have recently reported the chemistry of a simple tetradentate N_2S_2 ligand, *N,N'*-bis(mercaptoethyl)-1,5-diazacyclooctane (bme-daco), which strongly binds divalent transition metal ions and whose steric bulk fortunately inhibits aggregation in the case of nickel, producing the monomeric, square planar, thiolate complex (bme-daco)Ni^{II} (**1**).[10] Chemically simple modifications based on the nucleophilicity of the cis thiolate sulfur sites dramatically alter the redox behavior of Ni^{II} while maintaining N_2S_2 binding at distances commensurate with those suggested by EXAFS studies on NiFe hydrogenases (e.g., for *T. roseopersicina*, EXAFS data suggests 3 ± 1 N (O) at 2.06 Å and 2 ± 1 S (Cl) at 2.21 Å).[7c] Alkylation produces thioethers, and oxygenation of the thiolate sulfurs, either with hydrogen peroxide or by direct O_2 addition, has been shown to generate nickel-bound sulfinates.[12] Although sulfinates have not been proposed as biological ligands, they are of interest in regard to the deactivation of NiFe hydrogenases by oxygen.[13] Herein are reported redox potential data for a structurally characterized homologous series of six complexes, in which the sulfur sites are systematically varied in donor ability: thiolate (RS^-), thioether (RSR), sulfinate (RSO_2^-), and mixtures of these (Scheme I).

Experimental Section

General Methods. Solvents were reagent grade and were purified according to published procedures.[14] Sodium borohydride ($NaBH_4$), tetrabutylammonium hexafluorophosphate (TBAHFP), tetraethylammonium perchlorate (TEAP), methyl viologen dichloride ($MeVCl_2$), cerium ammonium nitrate (CAN), and methyl iodide (MeI) were used as obtained from Aldrich Chemical. Where anaerobic manipulation was required, an argon glovebox or standard Schlenk techniques were employed. Elemental analyses were performed by Galbraith Labs, Knoxville, TN.

Physical Measurements. Cyclic voltammograms were obtained on a Bioanalytical Systems 100A electrochemical analyzer with a glassy carbon stationary microelectrode and a platinum wire auxiliary electrode, using instrumental *iR* drop correction. Measurements in CH_3CN used 0.1 M [*n*-Bu_4N][PF_6] (TBAHFP) as supporting electrolyte and a vycor-tipped $Ag/AgNO_3$ reference electrode. For aqueous solutions a vycor-tipped Ag/AgCl reference electrode and 0.1 M KCl supporting electrolyte were used. Mixed-solvent experiments used 0.1 M TEAP solutions of both CH_3CN and H_2O and a glass-frit Ag/AgCl reference electrode. To correct for liquid junction potential differences, all potentials were scaled to the NHE reference using the $MeV^{2+/+}$ ($E_{1/2}^{NHE}$ = −440 mV)[15] as standard. The difficulty in comparing potentials between solvents is well documented.[16] The choice of the 2+/+ methyl viologen couple as reference was based on its reversibility in both CH_3CN and H_2O as well as its common application as a redox indicator in hydrogenase assays.[15b] The measured potential difference between Cp_2Fe/Cp_2Fe^+ and $MeV^{2+/+}$ in CH_3CN was 815 mV (the literature value for Cp_2Fe/Cp_2Fe^+ is $E_{1/2}^{NHE}$ = +400 mV in CH_3CN).[16b] In the mixed-solvent experiments, the potential difference between Cp_2Fe/Cp_2Fe^+ and $MeV^{2+/+}$ was constant in all mixtures in which Cp_2Fe remained soluble (0–40% H_2O).

EPR spectra were recorded on a Bruker ESP 300 equipped with an Oxford ER910A cryostat operating at 10 K. An NMR gaussmeter (Bruker ERO35M) and Hewlett Packard frequency counter (HP5352B) were used to calibrate the field and microwave frequency, respectively. Samples were typically 0.2 mM in analyte in MeOH or CH_3CN, frozen in liquid N_2 and then cooled to 10 K for analysis. *Warning: Frozen MeOH solutions in EPR tubes have exploded upon removal from liquid N_2.* UV–vis spectra were recorded on a Hewlett Packard 8452A diode array spectrophotometer. NMR paramagnetic shift determinations were recorded on a Varian XL-200 FT-NMR at 293 K.

Crystal examination, cell determination, and data collection were performed on a Siemens R3m single-crystal X-ray diffractometer using P3VAX 3.42 software. All crystallographic calculations were performed with SHEXTL-PLUS version 4.11 (G. M. Sheldrick, Institüt für Anorganische Chemie der Universität, Tammannstasse 4, d-3400, Gottingen, Germany) supplied by Siemens Analytical X-ray Instruments, Madison, WI.

Syntheses. The syntheses of (bme-daco)Ni^{II} (**1**),[10] *N,N'*-bis(3-thiabutyl)-1,5-diazacyclooctanenickel(II) diiodide, ([(btb-daco)Ni][I]$_2$, **6**),[10] and the sulfinates [*N*-(mercaptoethyl)-*N'*-(sulfinoethyl)-1,5-diazacyclooctanato]nickel(II) ((mese-daco)Ni^{II}, **2**),[12] and [*N,N'*-bis(sulfinoethyl)-1,5-diazacyclooctanato]nickel(II) ((bse-daco)Ni^{II}, **3**)[12] have been described elsewhere.

[*N*-(Mercaptoethyl)-*N'*-(3-thiabutyl)-1,5-diazacyclooctanato]nickel(II) Iodide [(metb-daco)Ni][I], 4).[17] A 0.10 g (0.34 mmol) sample of **1**, purified by column chromatography (silica gel, 95% EtOH eluent) and recrystallized from acetone/pentane, was dissolved in 25 mL of CH_3CN and treated with 1 equiv (21.4 μL) of MeI. The color of the solution immediately changed from purple to brown to orange. A small amount of solid precipitate was removed by filtration through Celite. Rotary evaporation to reduce the volume of the filtrate by half was followed by Et_2O diffusion to afford the product as red-brown crystals. A second crop from the supernatant brought the yield to 0.11 g, 74%. A red-brown parallelepiped, 0.34 × 0.48 × 0.60 mm, was chosen for single-crystal X-ray diffraction study. Anal. Calcd (found) for $C_{11}H_{23}N_2S_2NiI$: C, 30.51 (30.70); H, 5.35 (5.54); N, 6.47 (6.45).

[*N*-(Sulfinoethyl)-*N'*-(3-thiabutyl)-1,5-diazacyclooctanato]nickel(II) Iodide ([(setb-daco)Ni][I], 5). Complex **2** (67 mg, 0.69 mmol) was dissolved in 100 mL of CH_3OH. A total of 100 μL (in five 20-μL portions) of MeI (1.53 mmol) was added, and the solution color changed from brown-orange to yellow. On addition of Et_2O a yellow powder precipitated

(9) Ashby, M. T.; Enemark, J. H.; Lichtenberger, D. L. *Inorg. Chem.* **1988**, *27*, 191.

(10) Mills, D. K.; Reibenspies, J. H.; Darensbourg, M. Y. *Inorg. Chem.* **1990**, *29*, 4364. In this paper [(btb-daco)Ni][I]$_2$ was referred to as [(Me_2BME-DACO)Ni]I_2.

(11) Maroney, M. J.; Colpas, G. J.; Bagyinka, C.; Baidya, N.; Mascharak, P. K. *J. Am. Chem. Soc.* **1991**, *113*, 3962.

(12) Farmer, P. J.; Solouki, T.; Mills, D. K.; Soma, T.; Russell, D. H.; Reibenspies, J. H.; Darensbourg, M. Y. *J. Am. Chem. Soc.* **1992**, *114*, 4601.

(13) Kumar, M.; Colpas, G. J.; Day, R. O.; Maroney, M. J. *J. Am. Chem. Soc.* **1989**, *111*, 8283.

(14) Gordon, A. J.; Ford, R. A. *The Chemist's Companion*; Wiley and Sons: New York, 1972; pp 429–436.

(15) (a) Bird, C. L.; Kuhn, A. T. *Chem. Soc. Rev.* **1981**, *10*, 49. (b) Yagi, T.; Endo, A.; Tsugi, K. *Hydrogenases: Their Catalytic Activity, Structure and Function*; Schilgel, H. G., Schneider, K., Eds.; Erich Goltze KG: Gottingen, Germany, 1978; pp 107–127.

(16) (a) Headridge, J. B. *Electrochemical Techniques for Inorganic Chemists*; Academic Press: London and New York, 1969; pp 71–74. (b) Gagne, R. R.; Koval, C. A.; Lisensky, G. C. *Inorg. Chem.* **1980**, *19*, 2854. (c) Robinson, R. A.; Stokes, R. H. *Electrolyte Solutions*; Butterworth & Co., Ltd.: London, 1970 (revised); pp 351–357.

(17) Mills, D. K. Ph.D. Dissertation, Texas A&M University, 1991.

Table I. Experimental Data for the X-ray Crystal Structures of (bse-daco)Ni·H_2O (**3**), [(Metb-daco)Ni][I] (**4**), and [(setb-daco)Ni][I] (**5**)

complex	**3**	**4**	**5**
chemical formula	$C_{10}H_{22}N_2O_5S_2Ni$	$C_{11}H_{23}N_2S_2NiI$	$C_{11}H_{23}N_2O_2S_2NiI$
formula weight (g/mol)	373.1	465.1	433.06
space group	orthorhombic	triclinic	monoclinic
	$P2_12_12$ (No. 18)	$P\bar{1}$ (No. 2)	$P2_1/n$ (No. 14)
a, (Å)	8.696(4)	7.558(5)	9.012(2)
b, (Å)	9.993(5)	8.922(7)	12.891(3)
c, (Å)	8.015(4)	12.559(9)	14.055(3)
α (deg)		102.79(6)	
β (deg)		95.05(6)	99.42(2)
γ (deg)		107.23(6)	
V, (Å^3)	696.5(5)	778.0(10)	1610.8(6)
Z	2	2	4
ρ (calcd), (g cm^{-3})	1.779	1.849	1.909
temp (K)	193	193	193
radiation		Mo Kα (λ = 0.710 73 Å)	
absorption coefficient (mm^{-1})	1.705	3.458	3.355
min/max transmission coeff	0.933/0.985	0.5636/0.9061	0.6208/0.999
R (%)[a]	6.5	4.4	4.2
R_w (%)[a]	7.1	5.6	6.4

[a] Residuals: $R = \Sigma|F_o - F_c|/\Sigma F_o$; $R_w = \{[\Sigma w(F_o - F_c)^2]/[\Sigma w(F_o)^2]\}^{1/2}$.

and was collected by filtration; yield 83 mg (86%). Orange crystals were grown by Et_2O diffusion into a concentrated CH_3CN solution of **5**. A needle, 0.26 × 0.30 × 0.60 mm, was chosen for single-crystal X-ray diffraction study. FTIR peaks assigned to ν(SO) (KBr pellet): 1195, 1045 cm^{-1}. Anal. Calcd (found) for $C_{11}H_{23}N_2O_2S_2NiI$: C, 28.4 (28.7); H, 4.98 (5.04).

Ion Exchange of I^- by BF_4^-. For [(btb-daco)Ni][BF_4]$_2$ (**6′**), complex **6** (105 mg, 0.183 mmol) was dissolved in 100 mL of CH_3OH, and a solution containing $AgBF_4$ (68 mg, 0.364 mmol) in 50 mL of MeOH was transferred into it under an N_2 atmosphere. The color change from green to red was accompanied by formation of an off-white precipitate. Filtration twice through Celite yielded a clear red solution which was rotovaporated to a red solid, redissolved in 10 mL of CH_3CN, and recrystallized by slow Et_2O diffusion. The purple crystals thus obtained changed to red upon removal of solvent, yield 75 mg (83%). Anal. Calcd (found) for $C_{12}H_{26}N_2S_2NiB_2F_8$ C, 29.1 (29.4); H, 5.25 (5.22). Similar procedures were used for the conversions of [(metb-daco)Ni][I] (**4**) to [(metb-daco)Ni][BF_4] (**4′**) (brown powder obtained in 83% yield), and [(setb-daco)Ni][I] (**5**) to [(setb-daco)Ni][BF_4], (**5′**) (yellow, hygroscopic powder obtained after repeated washing with dry Et_2O in 66% yield). Ion exchange was confirmed by the lack of iodide oxidation waves in cyclic voltammograms of **4′**, **5′**, and **6′** (Figure 7).

Reductions with $NaBH_4$. Typically 0.10 g (0.17–0.31 mmol) of the reactant Ni^{II} complex was placed in a Schlenk flask and dissolved in 30 mL of thoroughly degassed, distilled MeOH under an N_2 atmosphere. Twenty milligrams (0.53 mmol) of $NaBH_4$ was dissolved in 20 mL of degassed distilled MeOH in an addition funnel, and 1 equiv was slowly added to the solution of the Ni^{II} complex. The color change to dark green was characteristic of all the reduced Ni solutions except **6**, which changed from green to tan. A black precipitate formed if an excess of borohydride was added. Immediately upon color change a 500-μL sample was transferred to a 5-mm quartz tube, frozen at −78 °C, and later cooled to −196 °C for EPR analysis.

Oxidation of (bse-daco)Ni^{II} (3). A 32-mg (90 μmol) sample of **3** was placed in a Schlenk flask and dissolved in 20 mL of thoroughly degassed, distilled MeOH under an N_2 atmosphere. Five milliliters (1 equiv) of an 18 mM solution of CAN in MeOH was added by cannula. The yellow solution immediately turned blue, but within seconds returned to yellow. Continued addition of the CAN solution (more than 5 equiv were added) had the same effect; with each drop, the solution changed to blue for a few seconds. An EPR sample of the blue product was obtained by placing 200 μL of the reactant solution into a 5-mm tube, transferring by cannula the CAN solution on top, and immediately freezing in liquid N_2 as the solutions mixed by diffusion.

Magnetism. Solution magnetisms for complexes **2–5** were determined by the Evans' method, which involves measuring the shift in ^{1}H NMR spectra induced by the presence of known amounts of the paramagnetic species.[18] Compounds **2**, **4**, and **5** were dissolved to ~0.02 M in 5% C_6H_6/CD_3OD; compound **3**, because of its reduced solubility in MeOH, was dissolved to ~0.02 M in 5% CH_3CN/D_2O. A microcell, coaxial sample tube of the solvent mixture was used as an external standard.

(18) Evans, D. F. *J. Chem. Soc.* **1959**, 2003.

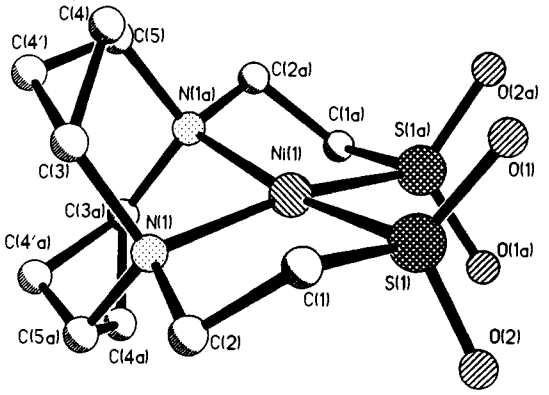

Figure 1. Molecular structure of (bse-daco)Ni·H_2O (**3**) less the lattice H_2O. Atoms labeled **a** are generated by a C_2 from refined atoms; hydrogen atoms have been omitted for clarity. Site occupancy for C(4) was refined to 46%, and for C(4′) to 56%. Selected bond lengths (Å): Ni(1)–S(1) 2.133(3); Ni(1)–N(1) 1.981(9); S(1)–O(1) 1.45(1); S(1)–O(2) 1.472(8); S(1)–C(1) 1.81(1). Selected bond angles (deg): S(1)–Ni(1)–S(1A) 92.6(2); N(1)–Ni(1)–N(1A) 89.7(5); N(1)–Ni(1)–S(1) 89.9(3); N(1)–Ni(1)–S(1A) 168.5(3); Ni(1)–S(1)–C(1) 99.0(4); Ni(1)–S(1)–O(1) 113.8(4); Ni(1)–S(1)–O(2) 115.3(3); O(1)–S(1)–O(2) 114.4(6).

Calculations were done as in ref 19, except for a correction for superconducting solenoidal field.[20] Results are given in Table II.

X-ray Structure Determinations. Large brown crystals of (bse-daco)Ni (**3**) were obtained as a monohydrate by layering a concentrated aqueous solution under dry acetone. A parallelepiped, 0.20 × 0.30 × 0.22 mm, was chosen for single-crystal X-ray diffraction study. Crystals of [(metb-daco)Ni][I] (**4**) and [(setb-daco)Ni][I] (**5**) suitable for X-ray studies were obtained as described above. Cell parameters and a summary of the data collection for all compounds are contained in Table I. Full structure reports are deposited as supplementary material, along with packing diagrams of complexes **3**, **4**, and **5**. Disorder is seen in all three structures, and the models used to refine the structures to convergence are expressed in the captions of Figures 1, 2, and 3 for **3**, **4**, and **5**, respectively.

Results

Syntheses. The syntheses of four members of the series to be discussed have been published.[10,12] The asymmetrical, monomethylated complex **4** could be obtained pure by the reaction described in eq 1 only if chromatographically pure **1** was used as starting material.[17] Otherwise mixtures of mono- and dimethylated complexes were obtained. The brown crystalline solid is air stable, however **4** reacts slowly with H_2O_2 to produce some of the oxygenate, complex **5**, along with unidentified

(19) Crawford, T. H.; Swanson, J. *J. Chem. Educ.* **1971**, *48*, 382.
(20) Live, D. H.; Chan, S. I. *Anal. Chem.* **1970**, *42*, 791.

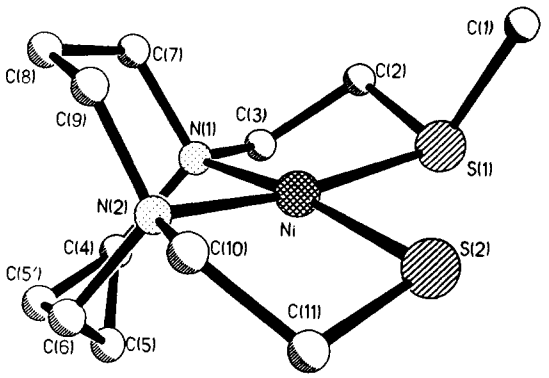

Figure 2. Molecular structure of [(metb-daco)Ni][I] (**4**) less the nonbonded anion; hydrogen atoms have been omitted for clarity. Site occupancy for C(5) was refined to 71%, and for C(5′) to 29%. Selected bond lengths (Å): Ni–S(1) 2.173(2); Ni–S(2) 2.155(3); Ni–N(1) 1.982(6); Ni–N(2) 1.935(5); S(1)–C(1) 1.797(7); S(1)–C(2) 1.816(9); S(2)–C(11) 1.813(8). Selected bond angles (deg): S(1)–Ni–S(2) 89.4(1); N(1)–Ni–N(2) 90.6(2); N(1)–Ni–S(1) 90.2(2); N(2)–Ni–S(2) 91.1(2); N(1)–Ni–S(2) 171.5(1); N(2)–Ni–S(1) 171.3(1); Ni–S(1)-C(1) 107.9(2); Ni–S(1)–C(2) 97.7(2); Ni–S(2)–C(11) 97.0(3).

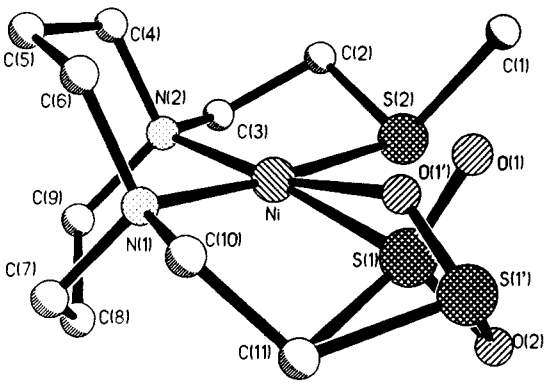

Figure 3. Molecular structure of [(setb-daco)Ni][I] (**5**) less the nonbonded anion; hydrogen atoms have been omitted for clarity. Site occupancy for S(1) and O(1) was refined to 92%, and for S(1′) and O(1′) to 8%. Selected bond lengths (Å): Ni–S(1) 2.142(2); Ni–S(2) 2.159(2); Ni–O(1′) 1.95(4); Ni–N(1), 1.978(5); Ni–N(2), 1.998(5); S(1)–O(1) 1.458(5); S(1)–O(2) 1.476(5); S(1′)–O(1) 1.41(2); S(1)–O(1′) 1.33(5); S(1′)–O(2) 1.40(2); S(2)–C(1) 1.819(6); S(2)–C(2) 1.820(7); S(1)–C(11) 1.825(7); S(1′)–C(11) 1.84(2). Selected bond angles (deg): S(1)–Ni–S(2) 91.6(1); N(1)–Ni–N(2) 91.0(2); N(1)–Ni–S(1) 88.2(2); N(2)–Ni–S(2) 89.7(2); N(1)–Ni–O(1′) 89(1); N(1)–Ni–S(2) 174.3(1); N(2)–Ni–S(1) 174.3(1); Ni–S(2)–C(1) 108.7(2); Ni–S(2)–C(2) 97.6(2); Ni–S(1)–C(11) 98.9(2); Ni–S(1)–O(1) 111.3(2); Ni–S(1)–O(2) 116.2(3); O(1)–S(1)–O(2) 116.1(3); O(1′)–S(1′)–O(2) 95(2).

$$\underset{\mathbf{1}}{\text{(bme-daco)Ni}^{\text{II}}} + \text{MeI} \rightarrow \underset{\mathbf{4}}{\text{[(metb-daco)Ni][I]}} \quad (1)$$

$$\underset{\mathbf{2}}{\text{(mese-daco)Ni}^{\text{II}}} + \text{MeI} \rightarrow \underset{\mathbf{5}}{\text{[(setb-daco)Ni][I]}} \quad (2)$$

oxidation products. A more effective synthesis of **5**, and the method of choice for obtaining crystalline material for X-ray analysis, results from methylation of the monosulfinato complex **2**, eq 2. The two strong ν(SO) IR bands at 1195 and 1045 cm^{-1} in KBr pellets of **5** are only slightly shifted from those observed for **2**, 1182 and 1053 cm^{-1}.[12]

Molecular Structures of 3, 4, and 5. The molecular structures of (bse-daco)Ni ($3{\cdot}H_2O$), [(metb-daco)Ni][I] (**4**), and [(setb-daco)Ni][I] (**5**) as determined by X-ray crystallography are shown in Figures 1, 2, and 3, respectively, and selected bond lengths and bond angles are given in the figure captions. As in the other complexes of Scheme I, the coordination environment about nickel is by and large square planar in **3**, **4**, and **5**, with a distortion toward a tetrahedral twist occurring to the greatest extent in **3** and to the smallest extent in **6**. Table II compares bond distance data and Td-twist angles for the six members of the series in Scheme I.[21]

Complex **3** shows disorder in the daco framework, as indicated in Figure 1. On the basis of the predominance of chair/boat configurations in the fused metalladiazacyclohexane rings of complexes of daco and derivatives,[22] that disorder is interpreted as arising from a near equal mixture of molecules which correlate C(4) with C(4′a) and C(4′) with C(4a). Nevertheless, previous structural analyses of daco complexes and derivatives have identified exclusive examples of the chair/chair as well as the chair/boat configuration; the former has always been found in six-coordinate complexes.[23] The disorder in complex **1** was attributed to a 50:50 distribution of chair/chair and chair/boat configurations, consistent with MM2 calculations, which find insignificant energy differences between the two forms.[23] Contribution to the disorder in **3** from a boat/boat configuration, a higher energy structure according to the MM2 calculations, cannot be ruled out; however it is considered less likely on the basis of structural precedents.

Complex **3** crystallizes with a water of hydration, shown in Figure 4, which hydrogen bonds to sulfinato oxygens between adjacent molecules with O···O distances of 2.814(5) Å. The packing diagram of **3** also shows molecules stacked head to tail with SO_2 units nestled into the daco moiety cleft of a second molecule.

The packing diagram of [(metb-daco)Ni][I] (**4**) indicates a long-range (3.88(1) Å) attraction between nickel and a thioether sulfur of an adjacent ion which gives rise to a weakly interacting unit containing a 2Ni2(R_2S) core (a parallelogram with ∠S–Ni–S = 65.7°), as seen in Figure 5. The angle between the 2Ni2(R_2S) core plane and the two parallel best-fit NiN2S2 planes is 92.7°. Related dimeric units in the bme-daco complexes of iron[24] and zinc[25] were found to employ thiolate sulfurs to form strongly bound 2M2(RS^-) cores. The dimeric stacking between Ni and the thioether sulfurs rather than thiolate sulfurs in **4** was unexpected due to the poorer Lewis basicity of thioethers. The daco ring of **4** also shows disorder, resulting from a mixture of chair/boat (71%) and chair/chair conformations of the metalladiazacyclohexane rings. There is no indication that intermolecular contacts promote the chair/chair conformations. Indeed, in the strongly bound dimer $[(\text{bme-daco})\text{Fe}]_2$, the chair/boat conformation is 100%.[24] Since the bis(thioether) **6** shows exclusively the chair/boat conformation and the parent dithiolate (**1**) a 50:50 mixture of chair/boat:chair/chair,[10] the monothioether derivative **4** would appear to be structurally intermediate between **1** and **6**.

As illustrated in Scheme I, the $[(\text{btb-daco})\text{Ni}][\text{I}]_2$ (**6**) complex shows both methyl substituents on the same side of the N_2S_2Ni plane, positioned so as to minimize cross-plane interactions with methylene CH_2 groups in the daco ring, as well as opposite a rather close interaction of one iodide counterion (Ni--I distance of 3.26 Å).[10] In [(metb-daco)Ni][I] (**4**) there is no such close ion pair interaction (the nearest iodide is at 4.725 Å) and the methyl group is on the same side of the plane as the chair

(21) The Td twist angles are measured as the angle of the intersection of the normals of the S(1)–X–S(2) and N(1)–X–N(2) planes, where X is the centroid of the N_2S_2 plane. As the nickel is not necessarily equidistant from the nitrogens and the sulfurs, the centroid rather than Ni is used to define the planes.

(22) (a) Legg, J. I.; Neilson, D. O.; Smith, D. L.; Larsen, M. L. *J. Am. Chem. Soc.* **1968**, *90*, 5030. (b) Neilson, D. O.; Larson, M. L.; Willet, R. D.; Legg, J. I. *J. Am. Chem. Soc.* **1971**, *93*, 5079. (c) Royer, D. J.; Schievelbein, V. H.; Kalyanaraman, A. R.; Bertrand, J. A. *Inorg. Chim. Acta* **1972**, *6*, 307.

(23) (a) Darensbourg, M. Y.; Font, I.; Mills, D. K.; Pala, M.; Reibenspies, J. H. *Inorg. Chem.* **1992**, *31*, 4965. (b) Goodman, D. C.; Tuntulani, T.; Farmer, P. J.; Darensbourg, M. Y.; Reibenspies, J. H. *Angew. Chem., Int. Ed. Engl.* **1993**, *32*, 116.

(24) Mills, D. K.; Hsiao, Y. M.; Farmer, P. J.; Atnip, E. V.; Reibenspies, J. H.; Darensbourg, M. Y. *J. Am. Chem. Soc.* **1991**, *113*, 1421.

(25) Tuntulani, T.; Reibenspies, J. H.; Farmer, P. J.; Darensbourg, M. Y. *Inorg. Chem.* **1992**, *31*, 3497.

Table II. Bond Lengths,[a] Tetrahedral Twist,[b] and Solution Magnetism[c]

compound (-daco)Ni	Ni–N (Å)		Ni–S (Å)	Td (deg)[b]	μ_{eff} (μ_B)[c]
1 bme-	1.979(7)		2.159(3)	13.2	0[a]
2 mese-	2.000(2) 1.982(2)	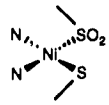	2.140(1) 2.163(1)	18.3	1.33
3 bse-	1.981(9)	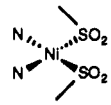	2.133(3)	15.9	1.23
4 metb- [I]	1.982(6) 1.935(5)	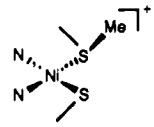	2.173(2) 2.155(3)	12.1	1.33
5 setb- [I]	1.998(5) 1.978(5)	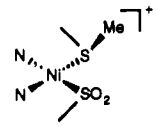	2.159(2) 2.142(2)	7.9	1.41
6 btb- $[I]_2$	1.974(7) 1.972(7)	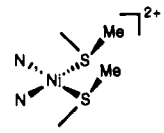	2.211(3) 2.204(3)	1.0	2.71[d]

[a] Structural data for **1** and **6** from ref 10, for **2** from ref 12, all others this work. [b] Calculated as described in ref 21. [c] In Bohr magnetons, determined by the Evans' method as described in ref 19. [d] From ref 10.

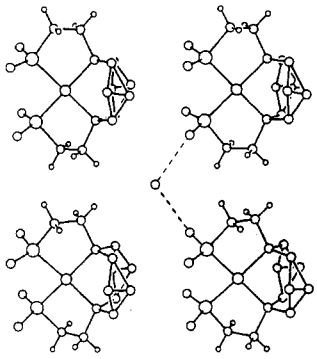

Figure 4. View projected along the *c* axis of the (bse-daco)Ni·H_2O (3·H_2O) crystal structure showing the H_2O of hydration hydrogen bonded between sulfinato oxygens of coplanar **3** molecules.

configuration of the NiN_2C_3 atoms. Likewise there is no close Ni--I^- interaction in [(setb-daco)Ni][I] (**5**). The similarity of the UV–vis spectra of both **4** and **5** with their BF_4^- salts, **4′** and **5′**, demonstrates the lack of ion pairing in solution (Table V).

Disorder in **5** is observed in the ambidentate nature of the sulfinato ligand. Thus 8% of the molecules exist in the O-bonded sulfinato form, and the remainder are S-bonded, as seen in Figure 3. An inversion at sulfur relates the two forms, with the position of one sulfinato oxygen unchanged. Interestingly, the major linkage isomer form has a slightly larger distortion from planarity (8° Td twist) than the minor form (4.3°).

Table II compares Ni–S and Ni–N bond distances for the six compounds in this series along with the tetrahedral twist angles, a measure of the degree of distortion of the NiN_2S_2 positions from a regular square plane, and the solution magnetisms as measured by the Evans' method. Of this series, only complex **1** is diamagnetic. Complex **6** shows the greatest paramagnetism, while for the remainder the magnetisms are on the order of 1–1.5 μ_B, i.e., less than the theoretical value for two unpaired electrons.

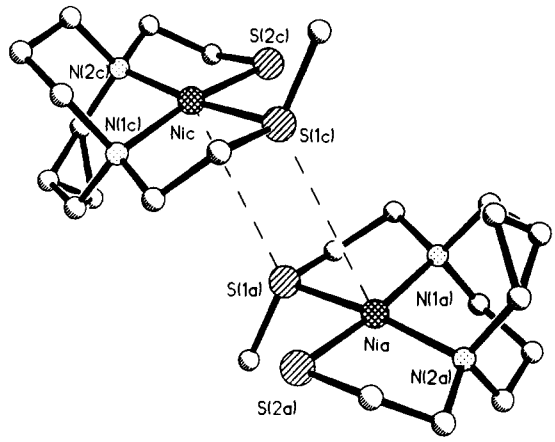

Figure 5. View of cation stacking in the [(metb-daco)Ni][I] (**4**) crystal structure illustrating long-range attraction in the 2Ni2(R_2S) unit.

Electrochemistry. Cyclic voltammograms for compounds **1**, **2**, and **3** in CH_3CN are found in Figure 6, while those of **4′**, **5′**, and **6′** are in Figure 7. A prominent feature common to all is a reversible reduction wave assigned (*vide infra*, EPR results) to the $Ni^{II/I}$ couple (Table III). Measurements in H_2O solution show voltammograms similar to those in CH_3CN within both solvent ranges; however the difference in redox potential of the $Ni^{II/I}$ couple between the various compounds is attenuated as compared to CH_3CN.

The reversibility of the reduction waves was poorer using a Pt working electrode, as contrasted to glassy carbon. This is ascribed to the affinity of sulfur-containing compounds for the heavy metal. Likewise, reversibility as measured by the i_{pa}/i_{pc} ratio was dependent on the degassing of the electrolyte solution; incomplete degassing led to loss of anodic peak current (all measurements were done under an N_2 blanket). The reversibility of the reduction waves of sulfinates **2** and **3** in H_2O was inversely dependent on

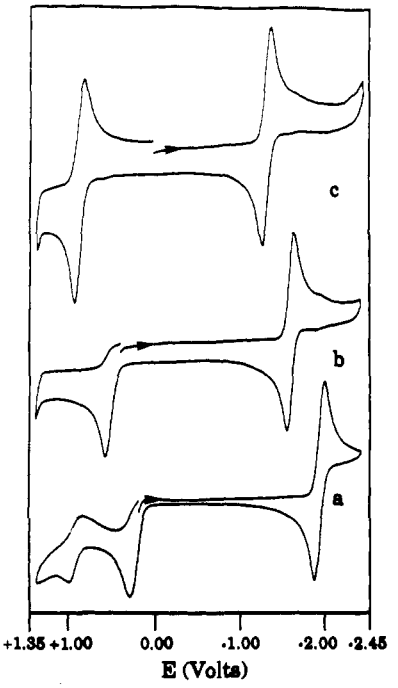

Figure 6. Cyclic voltammograms of 2–5 mM solutions of (a) (bme-daco)Ni (1), (b) (mese-daco)Ni (2), and (c) (bse-daco)Ni (3) in 0.1 M TBAHFP/MeCN with a glassy carbon working electrode at 200 mV/s; scale referenced to NHE using Cp_2Fe/Cp_2Fe^+ standard ($E_{1/2}$ = 400 mV).

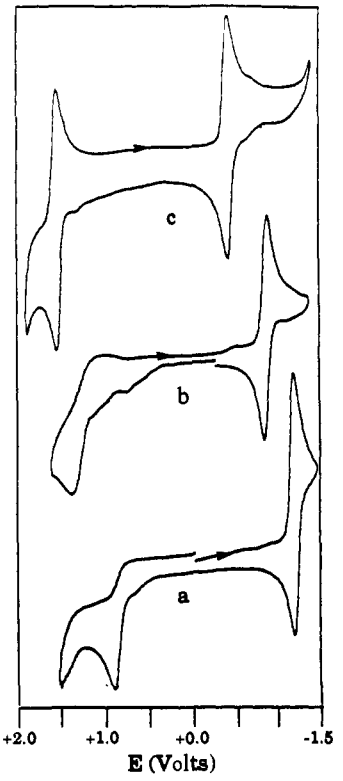

Figure 7. Cyclic voltammograms of 2–5 mM solutions of (a) [(metb-daco)Ni][BF_4] (4′), (b) [(setb-daco)Ni][BF_4] (5′), and (c) [(btb-daco)Ni][BF_4]$_2$ (6′) under conditions given in the caption for Figure 6.

scan speed, with the best values for 2 occurring at 25 mV/s (ΔE_p = 86, i_{pa}/i_{pc} = 0.52) and for 3 at 10 mV/s (ΔE_p = 108, i_{pa}/i_{pc} = 0.78), still quasi-reversible behavior.

An irreversible anodic wave was observed in the cyclic voltammograms of all compounds containing thiolate ligands (1, 2, and 4′), and the reverse scans following these waves produced smaller, broad cathodic waves resulting from the products of oxidation; approximate peak positions in CH_3CN are −230, −350, and −430 mV, respectively. This behavior for the monosulfinate 2 is shown in Figure 8. Scanning first through the irreversible anodic wave produces the broad wave on the following cathodic scan, but a cathodic scan from a potential below that of the anodic wave produces no such cathodic wave. There was no concentration dependence of the peak current ratio of (i_{pc} following wave)/(i_{pa} irreversible anodic wave) over concentrations of 3–0.03 mM 2 in CH_3CN.

EPR Measurements. Metal-centered reduction was supported by EPR of the products resulting from chemical (cobaltocene, $NaBH_4$, $LiHBEt_3$) reduction. For the dithioether 6, which has the highest reduction wave potential of the series, a variety of reductants, such as cobaltocene or Zn metal, can be used.[10] In order to chemically reduce compounds 2–5, a stronger reductant, $NaBH_4$ or $LiHBEt_3$, was necessary. Compound 1 decomposed upon reaction with $NaBH_4$ in MeOH to form the trinuclear Ni_3-(bme-daco)$_2^{2+}$ [12] and was unreactive with $LiHBEt_3$ in CH_3CN. Table IV gives the apparent g-values obtained on EPR analysis of the products resulting from $NaBH_4$ reduction of complexes 2–6, seen in Figure 9. The major feature in each spectrum is an axial signal with $g_{\parallel} > g_{\perp}$, typical of a d^9 system with one unpaired electron in the $d_{x^2-y^2}$ orbital. Other smaller, Ni-based signals were sometimes seen in addition to those described above. A second, isotropic signal is common in CH_3CN solutions of reduced 3 (g = 2.15), 5 (g = 2.11), and 6 (g = 2.06).[10] Lower field features are seen for 3 (g = 2.26, 2.12; see Figure 9) and 4 (g = 2.20, 2.16). The reduced products are extremely air sensitive, as implied by the sensitivity of i_{pa} to incomplete deaeration, and decompose under N_2 at room temperature within a short time (hours).

The EPR spectra of the product of chemical oxidation of 3 with CAN (Figure 10) display $g_{\parallel}$ (2.02) < $g_{\perp}$ (2.21), which denotes an octahedral d^7 ion with an unpaired electron in the d_{z^2} orbital.[26] The coordination of two solvent molecules has been proposed previously for square planar Ni complexes oxidized to Ni^{III}.[3,27] Complex 6′ was unaffected by CAN; $NOBF_4$ was unreactive with either 3 or 6′.

Discussion

The above series of complexes allows comparison of the σ- and π-donor ability of the thiolate, sulfinate, and thioether sulfur ligands in a relatively constant geometry. The π-antibonding interaction of a thiolate sulfur donor with an electronically satisfied or electron-rich metal such as d^8 Ni^{II} is substantially reduced on reaction with electrophiles such as H^+ or R^+.[9,28] Oxygenation of thiolate to sulfinato likewise binds the destabilizing lone pairs on sulfur, formally changes the oxidation state of sulfur from S^{-2}

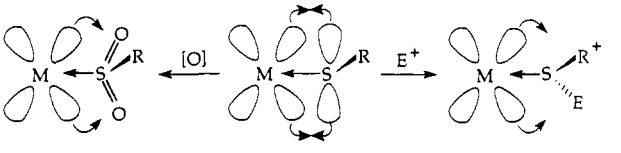

to S^{+2}, and yet maintains the sulfur donor ligand in anionic form. Previous to this study the electronic effect of these changes has been monitored in organometallic chemistry by the increase in ν(CO) stretching frequencies as the metal to CO π-back-bonding diminishes. The Cr–S distances in the $Cr(CO)_5$ pair of complexes

(26) (a) Maki, A. H.; Edelstein, N.; Davidson, A.; Holm, R. H. *J. Am. Chem. Soc.* **1964**, *86*, 4580. (b) Jacobs, S. A.; Margerum, D. W. *Inorg. Chem.* **1984**, *23*, 1195.

(27) (a) de Castro, B.; Freire, C. *Inorg. Chem.* **1990**, *29*, 5113. (b) Chavan, M. Y.; Meake, T. J.; Busch, D. H.; Kuwana, T. *Inorg. Chem.* **1986**, *25*, 314. (c) Krüger, H.-J.; Holm, R. H. *Inorg. Chem.* **1987**, *26*, 3645.

(28) Liaw, W.-F.; Kim, C.; Darensbourg, M. Y.; Rheingold, A. L. *J. Am. Chem. Soc.* **1989**, *111*, 3591.

Table III. Potential[a] and Reversibility Data from Cyclic Voltammetry in CH_3CN[b] (and H_2O)[c]

	complex reduction			complex oxidation			
compound (-daco)Ni	$E_{1/2}$ (mV)	ΔE (mV)	i_{pa}/i_{pc}	E_{pc} irrev	$E_{1/2}$ (mV)	ΔE (mV)	i_{pa}/i_{pc}
1 bme-	−1944	65	1.01	+360			
				(+543)			
2 mese-	−1631	70	0.97	+620			
	(−1067)[d]	(175)	(0.28)	(+939)			
3 bse-	−1339	72	0.93		+847	76	0.92
	(−761)	(125)	(0.65)				
4 metb- [I]	−1204	60	0.87	obscured[e]			
	(−962)	(62)	(0.80)				
4′ metb- [BF_4]	−1212	63	0.87	+956			
	(−962)	(75)	(0.75)	(+1105)			
5 setb- [I]	−930	64	0.92	+1290			
	(−577)	(76)	(0.98)				
5′ setb- [BF_4]	−939	64	1.01	+1280			
	(−580)	(71)	(0.78)				
6 btb- $[I]_2$	−482	72	0.98		+1568	76	0.97
	(−457)	(60)	(0.98)				
6′ btb- $[BF_4]_2$	−460	72	0.86		+1540	90	0.88
	(−450)	(66)	(0.83)				

[a] All potentials scaled to NHE referenced to a MeV^{2+}/MeV^{+} standard ($E_{1/2}^{NHE}$ = −440 mV). [b] In CH_3CN solutions, 0.1 M TBAHFP electrolyte, measured vs $Ag/AgNO_3$ reference electrode. [c] In H_2O solutions, 0.1 M KCl electrolyte, measured vs Ag/AgCl reference electrode. [d] On solvent reduction edge. [e] Oxidation peak obscured by those assigned to iodide counterion.

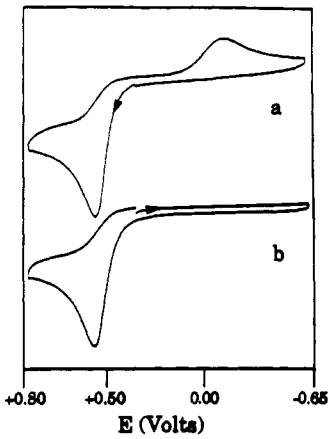

Figure 8. Cyclic voltammograms of (mese-daco)Ni (**2**) starting at +400 mV (a) scanning first toward positive potential and (b) scanning toward negative potential; conditions as in the caption for Figure 6.

Table IV. Apparent *g*-Values from EPR of Ni^I Products[a,b]

compound (-daco)Ni	$g_{\parallel}$	$g_{\perp}$	other signals[c]
2 mese-	2.21	2.070	2.23
3 bse-	2.18	2.058	2.26, 2.12 axial
4 metb- [I]	2.25	2.071	
5 setb- [I]	2.20	2.057	1.99, 1.93 broad
6 btb- $[I]_2$	2.24	2.066	2.10 isotropic

[a] Obtained by reduction of 1–2 mM solutions with $NaBH_4$ in MeOH. [b] X-band EPR, 10 K. [c] See text for discussion.

reflect the difference in p_π–d_π destabilization: Cr–S(thiol) = 2.439(2) Å and Cr–S(thiolate) = 2.479(2) Å.[29]

	$\Delta\nu$(CO) (cm^{-1})	ref
$PhSFe(CO)_4^-/(PhSMe)Fe(CO)_4$	+40	28
t-$BuSCr(CO)_5^-/(t$-$BuSH)Cr(CO)_5$	+35	29
$CpW(CO)_3SR/CpW(CO)_3SO_2R$	+20	30

In complexes **1**–**6**, the shortest Ni–S bonds are observed for Ni–SO_2R and reflect, in comparison to Ni–SR, the loss of p_π–d_π destabilization as well as the smaller radius of S^{2+} in SO_2R^- as compared to S^{2-} in SR^-. The N_2S_2 donor set is substantially square planar within the series, and likewise the metric data in Table II show a remarkable conformity in the N_2S_2 ligand cavity,

(29) Darensbourg, M. Y.; Longridge, E. M.; Payne, V.; Reibenspies, J.; Riordan, C. G.; Springs, J. J.; Calabrese, J. C. *Inorg. Chem.* **1990**, *29*, 2721.
(30) Weinmann, D. J.; Abrahamson, H. B. *Inorg. Chem.* **1987**, *26*, 3034.

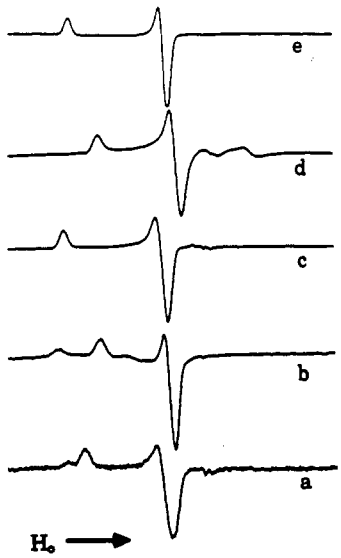

Figure 9. X-band EPR spectra obtained from MeOH solutions of (a) (mese-daco)Ni (**2**), (b) (bse-daco)Ni (**3**), (c) [(metb-daco)Ni][I] (**4**), (d) [(setb-daco)Ni][I], (**5**) and (e) [(btb-daco)Ni]$[I]_2$ (**6**) after reaction with <1 equiv of $NaBH_4$. All spectra obtained at 10 K, field strengths normalized for comparison.

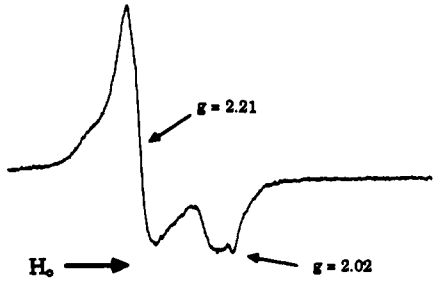

Figure 10. X-band EPR spectra obtained from an oxidized solution of **3**, as described in the text, in MeOH at 10 K.

in that the bond distances within the series of six complexes vary very little (ΔNi–N < 0.07 Å and ΔNi–S < 0.08 Å). A slight and variable distortion toward tetrahedral is observed in the crystal structures; however its effect on the electronic structure of Ni^{II} does not correlate with the observed magnetism. The only fully diamagnetic complex is **1**, which has a significant Td twist of 13.2°. The complex closest to planarity (**6**) is diamagnetic in the

Table V. Electronic Absorbances in the Visible Range for Ni^{II} Compounds

compound (-daco)Ni	CH_3CN λ_{max} (nm)	CH_3CN ϵ (mol^{-1} cm^{-3})	H_2O λ_{max} (nm)	H_2O ϵ (mol^{-1} cm^{-3})
1 bme-	506	640	522	130
	602 sh			
2 mese-	446	300	422	270
	554 sh		540 sh	
3 bse-	422	2140	388	770
			418	690
4 metb- [I]	460	130	478	130
	616 sh		580 sh	
4' metb- [BF_4]	467	120	476	145
	610 sh		580 sh	
5 setb- [I]	434	390	426	300
5' setb-[BF_4]	438	280	418	300
6 btb- $[I]_2$	428	930	490	125
	656	90	386 sh	
6' btb- $[BF_4]_2$	530	55	492	105
			390 sh	

Table VI. Effect of Oxygenation of a Thiolate Donor on $E_{1/2}$ for the $Ni^{II/I}$ Couple (in mV)

oxygenation	$\Delta E_{1/2}$ in CH_3CN	$\Delta E_{1/2}$ in H_2O
1 → **2**	+313	
2 → **3**	+292	+306
4 → **5**	+274	+385

Table VII. Effect of Methylation of a Thiolate Donor on $E_{1/2}$ for the $Ni^{II/I}$ Couple (in mV)

methylation	$\Delta E_{1/2}$ in CH_3CN	$\Delta E_{1/2}$ in H_2O
1 → **4**	+740	
4 → **6**	+722	+505
2 → **5**	+701	+490

solid state but displays concentration-dependent paramagnetism in solution.[10] The other four-coordinate complexes (**2–5**) show intermediate paramagnetism which is expected to involve spin equilibria.[31] A detailed description of the source(s) of paramagnetism is not possible at this time.

Effect of Oxygenations and Alkylations on the $Ni^{II/I}$ Potential. As given in Table III, the $Ni^{II/I}$ reduction potentials become more positive as the donor ability of the thiolate sulfurs is diminished. Tables VI and VII present this data in the form of differences resulting from oxygenation or alkylation of the sulfur site.

The shift in $Ni^{II/I}$ potential from the thiolate **1** to the monosulfinato complex **2** is ca. +310 mV in CH_3CN and corresponds to a 6.9 kcal/mol stabilization of the Ni^{I} state. The effect is additive in that oxygenation of **2** to the bis-sulfinato **3** also raises the potential by ca. +290 mV (Table VI). Further verification of this additivity is seen in the conversion of the thioether-thiolate complex **4** to the sulfinato-thioether complex **5**, which, once again, is accompanied by a potential increase of +275 mV. As there is no change in charge on the complex, this transformation is an accurate measure of the difference in donor ability of thiolate and sulfinate ligands, a reflection of both the change in sulfur formal oxidation state from 2^- to 2^+ and the resulting change in electron density at the metal.

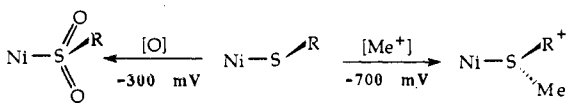

Alkylation of a thiolate site produces a much larger effect on the $Ni^{II/I}$ couple, as it affects both the donor ability of the sulfur

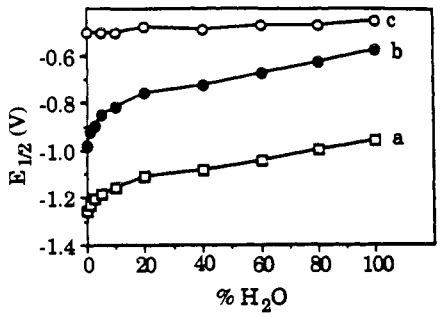

Figure 11. Plots of $E_{1/2}$ for the reduction waves of (a) [(metb-daco)Ni][I] (**4**), (b) [(setb-daco)Ni][I] (**5**), and (c) [(btb-daco)Ni]$[I]_2$ (**6**) vs % H_2O in 0.1 M TEAP H_2O/CH_3CN mixtures. Scaled to NHE using MeV^{2+}/MeV^{+} standard ($E_{1/2}$ = –440 mV).

site and the overall charge on the complex. Again the effect is additive, with the monothioether **4** couple separated by ca. 700 mV from the parent thiolate **1** as well as the dimethylated complex **6** in CH_3CN solution (Table VII). A 700-mV or 15.6 kcal/mol stabilization of the Ni^{I} state is likewise realized upon methylation of **2**, producing the mixed sulfinato/thioether **5**. The greatest stabilization of the lower oxidation state in CH_3CN is seen for the dicationic dithioether (**6**), a change of greater than 1400 mV, or over 31 kcal/mol, from the parent dithiolate (**1**).[32]

Hydrogen-Bonding Effects. The range of $Ni^{II/I}$ potentials in this series, measurable in both CH_3CN and H_2O for complexes **2–6**, is 1150 and 610 mV, respectively (Table III). This attenuation of the range of $Ni^{II/I}$ couples in H_2O is attributable to variable hydrogen bonding to the sulfur site ($SO_2R^- > SR^- >> SR_2$), which acts to decrease its σ-donor ability and increase its π-acceptor ability, thus stabilizing the reduced member of the redox couple.[33]

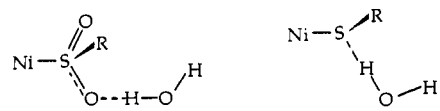

The neutral sulfinate complexes **2** and **3** are most susceptible to hydrogen bonding, as is seen in their higher solubilities in H_2O as compared to CH_3CN and definitively in the crystal structure of **3**, which shows such bonding between sulfinato oxygens and water (Figure 4). The $Ni^{II/I}$ potentials for **2** and **3** are greater than 500 mV more positive in H_2O than in CH_3CN. For the mixed sulfinato/thioether **5**, the stabilization in H_2O is ca. +350 mV; the loss of stabilization relative to the neutral sulfinates **2** or **3** denotes the decreased hydrogen-bonding ability of cationic species. For the thiolate/thioether **4** the stabilization is smaller, ca. +250 mV; the difference is attributable to a lessened effect on the donor character of thiolates compared to sulphinates. A greater hydrogen bonding is to be expected, and was observed, for negatively charged thiolate complexes; viz., a large shift (ca. 350 mV) in the $Ni^{III/II}$ couple of $[Ni(S_2\text{-norbornane})_2]^{2-}$, a dianionic tetrathiolate complex, was noted on going from CH_3CN to MeOH.[6]

A comparison of the relative hydrogen-bonding effects on sulfur donors is seen in Figure 11, which shows the $Ni^{II/I}$ potentials for (a) the thiolate/thioether **4**, (b) the sulfinate/thioether **5**, and (c) the dithioether **6**, determined in 0–100% H_2O in CH_3CN electrolyte mixtures. The $Ni^{II/I}$ couple for **6** is fairly constant

(31) Such equilibria are well documented. (a) Holm, R. H.; Chakravorty, A.; Theriot, L. J. *Inorg. Chem.* **1966**, *5*, 625. (b) Holm, R. H.; O'Connor, M. J. *Prog. Inorg. Chem.* **1971**, *14*, 241. (c) Sacconi, L.; Nannelli, P.; Nardi, N.; Campigli, U. *Inorg. Chem.* **1965**, *4*, 943.

(32) Iodide coordination[10] has only a small effect (–20 mV) on the $Ni^{II/I}$ couple, **6** as compared with **6'** (Table III). A much larger effect has been seen in similar compounds for the coordination of Br^- and Cl^-.[23] In H_2O, **6** and **6'** display similar behavior both electrochemically and spectroscopically (Tables III and V), implying both are in square planar environments.

(33) (a) Mascharak, P. K. *Inorg. Chem.* **1986**, *25*, 245. (b) Hill, C. L.; Renaud, J.; Holm, R. H.; Mortenson, L. E. *J. Am. Chem. Soc.* **1977**, *99*, 2549.

over the range of solvent mixtures as measured versus the $MeV^{2+/+}$ standard. In contrast, a dramatic shift occurs for **4** (+100 mV) and **5** (+170 mV) between 0 and 10% H_2O. A similar effect was seen for the $Fe^{III/II}$ couple in $(Et_4N)_3Fe(CN)_6$, which is over 600 mV more positive in a mixture of 9% H_2O/CH_3CN than in 100% CH_3CN.[33a]

The effects of alkylation or oxygenation on $Ni^{II/I}$ potentials in H_2O (Tables VI and VII) are readily explained in terms of hydrogen bonding. For alkylation, water decreases the $Ni^{II/I}$ potentials of the reactant thiolates, but not the product thioethers, thus lessening the difference from ~700 to ~500 mV. For oxygenation, the product sulfinates are more affected than the reactant thiolates. This effect is greatest for the cationic **4** where oxygenation to **5** raises the $Ni^{II/I}$ couple by 275 mV in CH_3CN and by 385 mV in H_2O. The difference is much smaller for the neutral pair **2** and **3**, in which there are two hydrogen-bonding sites in both the reactant and product.

Complex Oxidations. Reversible oxidation waves are seen for the bissulfinate **3** and the dithioether **6** (and **6'**). Since sulfur-based oxidations are unlikely in these compounds, this event was assigned to a $Ni^{II/III}$ couple, which was supported by EPR spectral analysis of chemically oxidized **3** (vide supra). Interestingly, the mixed thioether/sulfinate **5** does not show a reversible oxidation wave (Figure 7). For complexes **3** and **6**, which show reversible $Ni^{II/III}$ waves, as well as the other complexes which show irreversible oxidations, *vide infra*, the difference between oxidation features and reduction couples is ca. 2.0 V.

All complexes with thiolate donor sites (**1**, **2**, **4**, **4'**) undergo irreversible oxidations (Table III). Similar irreversible oxidation waves observed in other compounds containing thiolate ligands have been assigned to a sulfur-based oxidation (thiolate to thiyl radical) supported by chemical and electrochemical[34-36] studies, as well as crystal structures of the products of sulfur-based oxidation.[36,37] Likewise, the stoichiometry of chemical oxidations of **1** (eq 3) suggests a similar, sulfur-based oxidation. Here a

$$3(\text{bme-daco})\text{Ni} + I_2 \rightarrow [Ni_3(\text{bme-daco})_2][I]_2 + \text{ligand oxidized products} \quad (3)$$

two-electron oxidation of **1** produces free Ni^{2+}, which is rapidly trapped by two nonoxidized **1** complexes, forming the trinuclear species.[12]

The chemical nature of the unstable intermediates of Ni thiolate oxidation is less clear-cut: is it Ni^{III} or S radical? The range of these irreversible oxidation potentials, varying over 600 mV, belies their assignment as solely sulfur ligand-based phenomena. Certainly there is considerable covalency to the Ni–S bonds, and the Ni character of the oxidations is noted in the maintenance of a 2-V separation between oxidation and reduction waves, whether reversible or not. Despite such arguments for Ni involvement in the oxidations, the ultimate fate is apparently sulfur-ligand decomposition.

EPR, UV–vis Spectroscopy, and Magnetism. Whereas the electrochemistry of compounds **1–6** shows a direct correlation between the σ-donor ability of the sulfur ($RS^- > RSO_2^- > R_2S$) and $Ni^{II/I}$ couple potentials, attempts to correlate their Ni^I EPR signal positions suggest a different ordering. The observed symmetries (axial) and g-values ($g_\parallel$ = 2.18 – 2.25, and $g_\perp$ = 2.057 – 2.071) are quite similar. This indicates the d-orbital energies of the complexes are determined by similar ligand fields (i.e., coordination geometries similar to their solid-state, square planar structures). We have attempted to assign the relative ligand field strengths of the sulfur ligands RS^-, R_2S, and RSO_2^- from the EPR data. A simple analysis predicts the values of $g_\parallel$ should vary inversely with the relative ligand field strength (assuming no change in the spin-orbit coupling constant for the different complexes and insignificant mixing of metal $d_{x^2-y^2}$ and d_{xy} with ligand orbitals).[38] Comparison of the $g_\parallel$ values given in Table IV indicates the order of ligand field strengths to be $RSO_2^- > R_2S > RS^-$. This is congruent with the observed shifts in the electronic absorption spectra (Table V), where the highest energy absorptions are seen for the bissulfinate **3** and the lowest for the dithiolate **1** (the relative ligand field strength of R_2S has precedence in other spectrochemical series).[39] A better analysis of these trends demands a clearer understanding of the orbital energies and identification of the absorption transitions, thus necessitating solution structural information on the Ni^I as well as Ni^{II} species.

The magnetism of the series (Table II) more closely correlates with the electrochemistry. Of the compounds studied, **6** is the most easily reduced and has the greatest paramagnetism. Compound **1** is the most difficult to reduce and is the only one that is diamagnetic in solution. This suggests that the energy splitting between the d_{z^2} and $d_{x^2-y^2}$ orbitals of **1** is large, making $S = 0$ the ground state, whereas for **6** the splitting is small and $S = 1$ is the ground state. The remaining complexes (**2–5**) all exhibit effective magnetic moments intermediate between those expected for $S = 1$ and $S = 0$; the two spin states in these complexes are probably near in energy, and both are significantly populated at the temperature of the susceptibility measurements.

Summary and Comments

The electrochemistry of nickel in sulfur ligation depends on the S-donor ligands as follows:

Donor Character. The ability to stabilize Ni^I changes according to the substituents on S, varying in the series $SR^- < SO_2R^- < SR_2$. This is reflected in the electrochemistry of the $Ni^{II/I}$ process, i.e., the accessibility of the $Ni^{II/I}$ couple. Exchanging the sulfur-donor site within this series has a consistent and additive effect on nickel-based redox potentials. This consistency reflects regular changes in the electron density at the metal that are not necessarily mirrored in EPR or UV–vis spectroscopy.

Solvent Effects. Hydrogen bonding to the S-donor site stabilizes Ni^I in the series $SO_2R^- > SR^- >> SR_2$, by decreasing the donor ability of the sulfur (and thus destabilizing the Ni^{III} state). A rough estimate of such effects is ca. +250 mV for thiolate and ca. +350 mV for sulfinates. Electrochemical measurements in nonprotic solvents avoid these effects and are poor models for aqueous biological systems.

Oxidation Stabilities. Reversible oxidation waves were seen only for compounds without thiolate donors in our series of cationic and neutral complexes. The thiolate complexes undergo irreversible, apparently sulfur-based oxidations. Dianionic, sterically hindered Ni thiolates as demonstrated by Millar et al.[6] and Holm et al.[4] have a greater stability to oxidations, showing stable Ni^{III} products.

It is interesting to note that in tetraaza macrocyclic systems the more accessible redox couple is $Ni^{III/II}$,[3] whereas with our N_2S_2 compounds it is $Ni^{II/I}$. A crude comparison of the effect of N vs S coordination can be made using macrocyclic complexes **7**[3] and **8**[23] seen below. The difference in $Ni^{II/I}$ potentials of over 0.7 V is ascribed to the "softer" thioether's ability to stabilize the "softer" Ni^I.

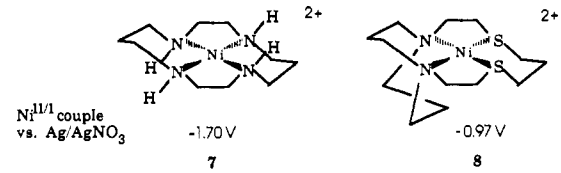

(34) Krüger, H. J.; Holm, R. H. *Inorg. Chem.* **1989**, *28*, 1148.
(35) Choudhury, S. B.; Ray, D.; Chakravorty, A. *Inorg. Chem.* **1990**, *29*, 4603.
(36) Springs, J.; Janzen, C. P.; Darensbourg, M. Y.; Calabrese, J. C.; Krusic, P. J.; Verpeaux, J.-N.; Amatore, C. *J. Am. Chem. Soc.* **1990**, *112*, 5789.
(37) Kumar, M.; Day, R. O.; Colpas, G. J.; Maroney, M. J. *J. Am. Chem. Soc.* **1989**, *111*, 5974.

The ubiquity of sulfur in the first coordination spheres of the redox-active nickel sites of hydrogenase enzymes may be to achieve this Ni^{I} state, which has been proposed to be integral to the catalytic cycle.[1b] Of the three common sulfur donors in biological systems (cysteinate, methionine, sulfide), the thioether methionine would best stabilize Ni^{I}. Preliminary results on polynuclear complexes using **1** as a metalloligand demonstrate a similar stabilizing effect for μ^2-bridging thiolates, which are metalated versions of thioethers.[25]

(38) Wertz, J. E.; Bolton, J. R. *Electron Spin Resonance Elementary Theory and Practical Applications*; Chapman and Hall: New York and London, 1986; Chapter 11.

(39) (a) Rosen, W.; Busch, D. H. *J. Am. Chem. Soc.* **1969**, *91*, 4694 and references therein. (b) Wieghardt, K.; Küppers, H.-J.; Weiss, J. *Inorg. Chem.* **1985**, *24*, 3067.

Acknowledgment. Financial support from the National Institutes of Health (Grant RO1 GM44865-01) is gratefully acknowledged. Funding for the EPR spectrometer (Grant CHE-8912763) and for the X-ray diffractometer and crystallographic computing system (Grant CHE-8513273) was provided by the National Science Foundation.

Supplementary Material Available: Tables of atom positional parameters, bond lengths and angles, and anisotropic displacement parameters and packing diagrams of (bse-daco)Ni·H_2O, [(metb-daco)Ni][I], and [(setb-daco)Ni][I] (16 pages); listings of structure factors for (bse-daco)Ni·H_2O, [(metb-daco)Ni][I], and [(setb-daco)Ni][I] (24 pages). Ordering information is given on any current masthead page.